Electronic and optical properties of substitutional V, Cr and Ir impurities in Cu_2ZnSnS_4

C. Tablero

The substitution of cation atoms by V, Cr and Ir in the natural and synthetic quaternary Cu_2ZnSnS_4 semiconductor is analyzed using first-principles methods. In most of the substitutions, the electronic structure of these modified CZTS is characterized for intermediate bands with different occupation and position within of the energy band gap. A study of the symmetry and composition of these intermediate bands is carried out for all substitutions.

These bands permit additional photon absorption and emission channels depending on their occupation. The optical properties are obtained and analyzed. The absorption coefficients are split into contributions from the different absorption channels and from the inter- and intra-atomic components. The sub bandgap transitions are significant in many cases because the anion states contribute to the valence, conduction and intermediates bands. These properties could therefore be used for novel optoelectronic devices.

1. Introduction

CZTS is a mineral which is found in nature and can be synthesized through solid-state chemical reactions between ZnS, Cu_2S, and SnS_2. The natural CZTS [1] contains a small amount of Fe. But iron-free CZTS can be synthesized [2]. The natural and synthetic CZTS differ slightly in their lattice parameters. A broad range of techniques have been explored to deposit CZTS films: sulfurization of sputtered [3–5] or evaporated [6] stacked films, spray method [7,8], sol–gel method [9], hydrazine deposition [10], and electrode deposition [11]. Their properties have been extensively studied both experimentally [12–19] and theoretically [20–23]. The experimental samples usually crystallize in kesterite-type structure because it is more stable thermodynamically than the stannite-type, although the stannite-type structure can be formed through a two step process [24].

In addition to the relatively abundant constituents, with low-cost and nontoxic, CZTS has potentially interesting properties for optoelectronic devices. Among these properties, the bandgap energy (1.4–1.6 eV) and high absorption coefficient ($\alpha \sim 10^4$ cm^{-1}) stand out. One of the purposes of modern solid-state chemistry and physics is to design and manufacture new materials with suitable properties to be used as optoelectronic devices. The insertion of intermediate states into the bandgap of a semiconductor material provides additional channels for optical transitions. For example, it could increase the efficiency of solar cell devices ($>60\%$) [25].

Some materials have attracted attention in the insertion of intermediate states using different host-impurity combinations: some transition-metal doped chalcopyrites [26–29], II–VI semiconductors doped with isoelectronic oxygen impurities, and Cr-doped zinc chalogenides [30,31]. The isoelectronic doping of II–VI compounds with oxygen has shown that oxygen gives rise to deep traps [32–35] at which carriers recombine radiatively [36–40]. Cr-doped zinc chalogenides [41–43] have been used as broadly tunable continuous wave lasers.

Because CZTS is one of the most promising materials for low-cost solar cell applications, and in order to further improve conversion efficiency, it is important to examine the effect of doping in these compounds. Previously, a general systematic ab initio study has been carried out using several transitions metals. From the results, V, Cr and Ir have been identified as interesting impurity candidates to obtain intermediate states within the main gap of the modified CZTS.

2. Calculations

We study the influence of the substitutional incorporation of M impurities into all cation A sites (M_A substitutions with A=Cu, Sn and Zn, and M=V, Cr and Ir) of CZTS on its electronic and optical properties using first principles within the density functional formalism [44,45]. For the exchange-correlation potential, we used

the generalized gradient approximation from Perdew, Burke and Ernzerhof [46]. The standard Troullier–Martins [47] pseudopotentials are adopted and expressed in the Kleinman–Bylander [48] factorized form. The valence wave functions are expanded into a numerically localized pseudoatomic orbital basis set [49].

The CZTS mainly crystallizes in the kesterite structure. Natural CZTS often contains Fe [2], although synthetic (iron-free) has been obtained experimentally [1]. The experimental lattice parameters are different: a_H=5.427 Å and $c_H/2a_H$=1.002 (HLP) for natural and a_S=5.485 Å and $c_S/2a_S$=0.997 (SLP) for synthetic CZTS. The M_{Cu}, M_{Zn}, and M_{Sn} substitutions ($(M_xCu_{2-x})ZnSnS_4$, $Cu_2(M_xZn_{1-x})SnS_4$ and $Cu_2Zn(M_xSn_{1-x})S_4$ respectively) are analyzed using 64-atom supercells (x=0.083) with periodic boundary conditions and spin polarization. In all of the results presented in this work 24 special k points in the irreducible Brillouin zone and a double-zeta with polarization localized basis set has been used for the 64-atom supercells.

From the energies $E_{\mu,\vec{k}}$ and occupations $f_{\mu,\vec{k}}$ of the μ bands at $\vec{k}$ points of the Brillouin zone obtained with band structure calculations, we have calculated the momentum matrix elements $p_{\mu\lambda}$ and the complex dielectric e_2 function according to:

$$e_2(E) \sim \frac{1}{E^2}\sum_{\mu}\sum_{\lambda}\int d\vec{k}\,|p_{\mu\lambda}|^2[f_{\mu,\vec{k}} - f_{\lambda,\vec{k}}]\delta(E_{\lambda,\vec{k}} - E_{\mu,\vec{k}} - E)$$

The other optical properties are obtained using the Kramers–Kronig relations. The $p_{\mu\lambda}$ elements can be split as $p_{\mu\lambda} = p^{(e)}_{\mu\lambda} + p^{(a)}_{\mu\lambda}$, where $p^{(a)}_{\mu\lambda}$ is the intra-atomic component that couples the localized basis set functions on the same atom, and $p^{(e)}_{\mu\lambda}$ is the inter-atomic component that couples basis set functions of different atoms. As the optical properties depend on the square of the momentum operator matrix elements, they can be separated into three terms: intra-atomic (depending on $|p^{(a)}_{\mu\lambda}|^2$), inter-atomic (depending on $|p^{(e)}_{\mu\lambda}|^2$), and a coupling term (depending on $|p^{(e)}_{\mu\lambda}||\,p^{(a)}_{\mu\lambda}|$).

3. Results and discussion

The host CZTS bandgap obtained using SLP for the 64- and 216-atom cells are 0.71 eV and 0.75 eV, respectively [50]. With the HLP these values are 0.96 eV and 0.95 eV. The main difference in the band structure between the HLP and SLP is a lower band gap when the SLP are used. These results present the well-known gap-underestimation problem with respect to the experimental data (1.4–1.6 eV [12–19]). Nevertheless, these results present a lower underestimation than other theoretical data in the literature with similar methods (~0.09 eV using the GGA [20,21]), although larger than more sophisticated hybrid functional methods (~1.5 eV [20,21]). However, more accurate first-principles approaches that partially avoid this band-gap underestimation problem are currently not practical in large supercells.

When V, Cr or Mn occupy cation host sites (M_{Cu}, M_{Zn}, and M_{Sn} substitutions, with M=V, Cr or Mn), one of the main effects in the electronic structure is to create intermediate bands (IB) within the energy bandgap. These IB are full, empty and partially-full depending on the substitutions. The Cr substitutions have been analyzed previously in the literature [50]. From the results, the IB within the energy bandgap is very similar for all substitutions. The main difference is a lower band gap when the SLP are used. In addition, the band structure for the two possible crystallographic non-equivalent Cr_{Cu} substitutions has only slight differences [50]. Thus, henceforth the two Cu sites are not differentiated.

According to the ionic model, when Cu, Zn or Sn host atoms are substituted by M, the M oxidation states are +1, +2 and +4: $M^{p+}(d^{n-p})$, p=1,2 and 4 for the M_{Cu}, M_{Zn}, and M_{Sn} substitutions, and n=5, 6 and 9 for M=V, Cr and Ir. Of course, the oxidization states proceed historically from the field of ionic compounds where the charge transfer is almost complete. In solids and molecules the bonding is in general not ionic. Thus, the atomic

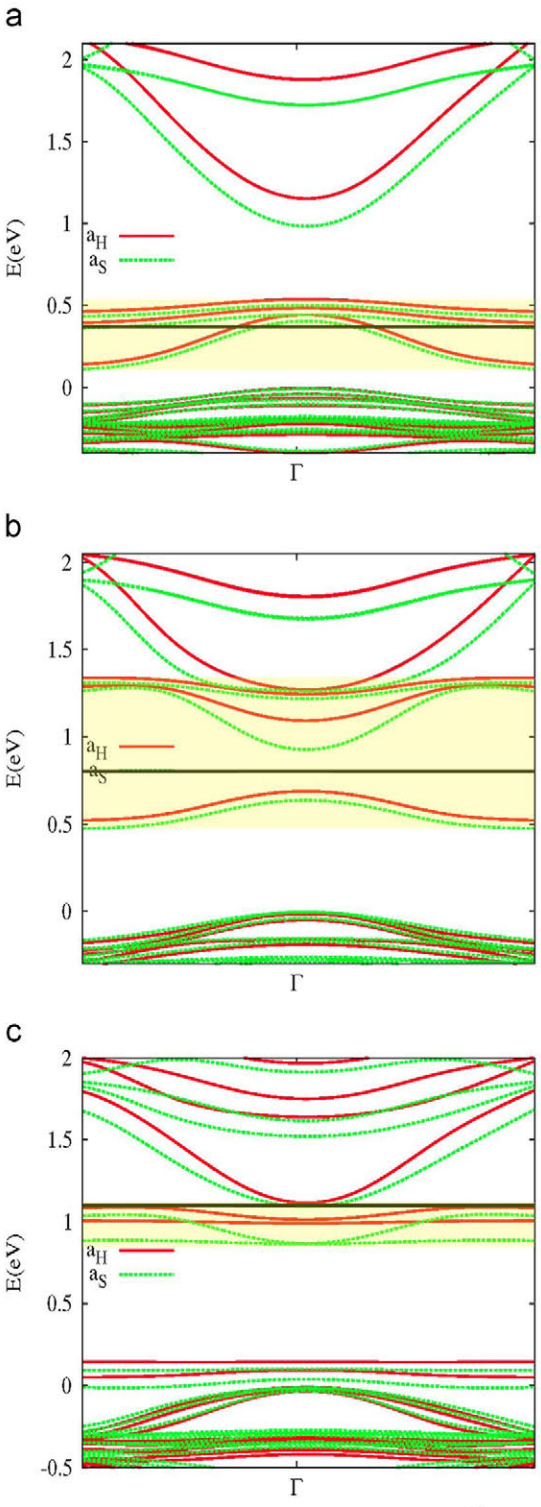

Fig. 1. Energy-band diagram around the Γ point in the BZ (from $-\vec{b}_3/2$ to $+\vec{b}_3/2$, where $\vec{b}_3$ is a reciprocal lattice vector) for the spin up component of the (a) Cr_{Zn}, (b) V_{Zn} and (b) V_{Cu} substitutions. The VB edge of the spin up component has been chosen as the energy origin. The horizontal line is the Fermi energy. The solid and dashed lines correspond to the HLP and SLP, respectively. The t-IB has been shadowed in the panels.

charge will not be +1, +4, and +2 either for Cu, Sn and Zn, or for an impurity when substituting to these host atoms.

The first shell of anions around the M atom is distributed with approximately tetrahedral symmetry. The d-M orbitals are split by the crystalline field into d_e-states (d_{z^2} and $d_{x^2-y^2}$) and d_t-states (d_{xy},d_{xz}, and d_{yz}). In addition to the crystalline field, the spin splits these states into two components, (+) for majority and (−) for the minority spin component. In the crystalline field with spin, the atomic electronic configurations at the tetrahedral substitutional site are:$V_{Cu}(d^2_{e+}\, d^2_{t+}\, d^0_{t-}\, d^0_{e-})$,$V_{Zn}(d^2_{e+}\, d^1_{t+}\, d^0_{t-}\, d^0_{e-})$, $V_{Sn}(d^1_{g+}\, d_t{}^{+0}d^0_{t-}\, d^0_{e-})$,$Cr_{Cu}(d^2_{e+}\, d^3_{t+}\, d^0_{t-}\, d^0_{e-})$, $Cr_{Zn}(d^2_{e+}\, d^2_{t+}\, d^0_{t-}\, d^0_{e-})$,$Cr_{Sn}(d^2_{e+}\, d_t{}^{+0}d^0_{t-}\, d^0_{e-})$,$Ir_{Cu}(d^2_{e-}\, d^2_{e+}\, d^3_{t+}\, d^1_{t-})$,$Ir_{Zn}(d^2_{e-}\, d^2_{e+}\, d^3_{t+}\, d^0_{t-})$, and $Ir_{Sn}(d^2_{e-}\, d^2_{e+}\, d^1_{t+}\, d^0_{t-})$.

The crystal wavefunctions with t and e symmetry are formed mainly through the combination of the d-M and the host states S states with the appropriate symmetry, mainly by the first shell of anions: $\mu_{\pm} \simeq a_{\mu\pm} \times d_{\mu\pm} + b_{\mu\pm} \times H_{\mu\pm}$, with μ=t,e, and the (+) and (−) sub-indexes indicate the spin polarization. Some of these functions are those that lead to states within the gap for the substituted CZTS. Nevertheless, as has already been mentioned, the local symmetry around the impurity atom is not exactly tetrahedral, either for the HLT or for the SLP. Therefore, the t and e states will not be pure. We refer to t and e states when the larger contribution is of the d_t-M or d_e-M states, respectively.

The electronic band configuration in the gap and in the edges of the VB and CB for the substitutions analyzed are: $V_{Cu}((e^2_+)[t^2_+](t^0_-\, e^0_-))$,$V_{Zn}((e^2_+)[t^1_+](t^0_-\, e^0_-))$,$V_{Sn}((e^1_+\, t^0_+)(t^0_-\, e^0_-))$, $Cr_{Cu}((e^2_+)[t^3_+](t^0_-\, e^0_-))$, $Cr_{Zn}((e^2_+)[t^2_+](t^0_-\, e^0_-))$, $Cr_{Sn}((e^2_+)(t^0_+\, t^0_-\, e^0_-))$, $Ir_{Cu}((e^2_-\, e^2_+)[t^3_+\, t^1_-])$, $Ir_{Zn}((e^2_-\, e^2_+)[t^3_+\, t^0_-])$, and $Ir_{Sn}((e^2_-\, e^2_+)[t^1_+\, t^0_-])$. In order to easily appreciate the contribution to the different energy

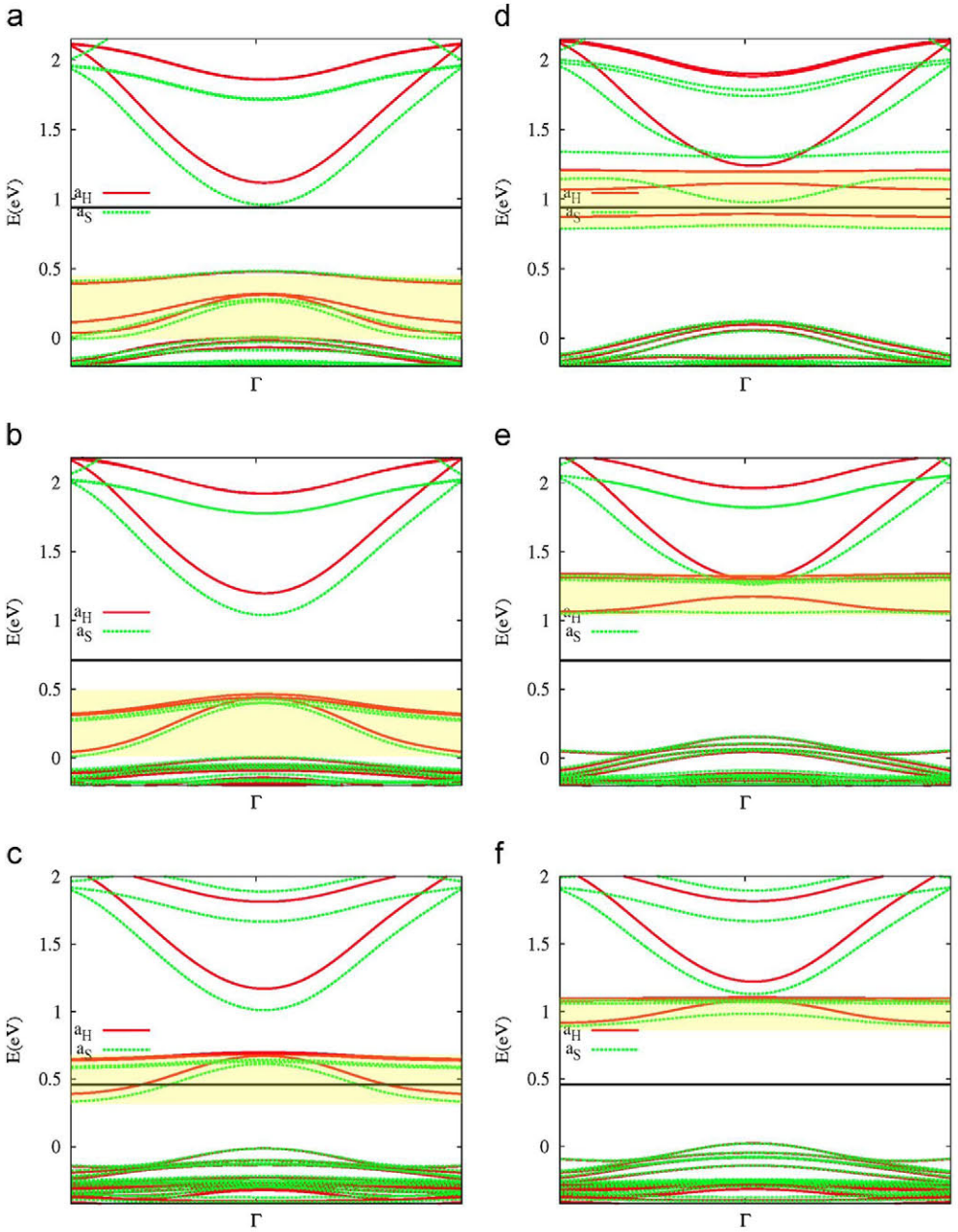

Fig. 2. Energy-band diagram around the Γ point in the BZ (from $-\vec{b}_3/2$ to $+\vec{b}_3/2$, where $\vec{b}_3$ is a reciprocal lattice vector) for the spin up component of the (a) Ir_{Cu}, (b) Ir_{Zn}, and (c) Ir_{Sn} CZTS substitutions. In the panels (d), (e) and (f) represent the spin down component for the Ir_{Cu}, Ir_{Zn}, and Ir_{Sn} substitutions respectively. The VB edge of the spin up component has been chosen as the energy origin. The horizontal line is the Fermi energy. The solid and dashed lines correspond to the HLP and SLP, respectively. The t-IB has been shadowed in the panels.

ranges, we have indicated the states in the band gap between square brackets, and the states within the VB and CB in round brackets. For the V_{Sn} substitution, the Fermi energy is in the VB because the e_+ state in the VB edge is not full. For the V and Cr, except for the V_{Sn} substitution, the IB is the t_+, e_+ is in the VB and t_- and e_- is in the CB. For Ir, both the t_+ and t_-, are IB in the gap, and t_- and e_- are in the VB. The electronic band structure, the projected density of states and the total magnetization of the unit cell per M atom obtained from the calculations are in agreement with these configurations.

The more interesting cases where there are partially-full bands in the band gap for the V and Cr substitutions are represented in Fig. 1. For all Ir substitutions, with two IB with different spins in the energy band gap, the results are shown in Fig. 2. The IBs in these figures have been shadowed in order to appreciate them more clearly. For the $V_{Zn}[t_+^1]$ and the $V_{Cu}[t_+^2]$ substitutions the partially-full t_+-IB overlaps

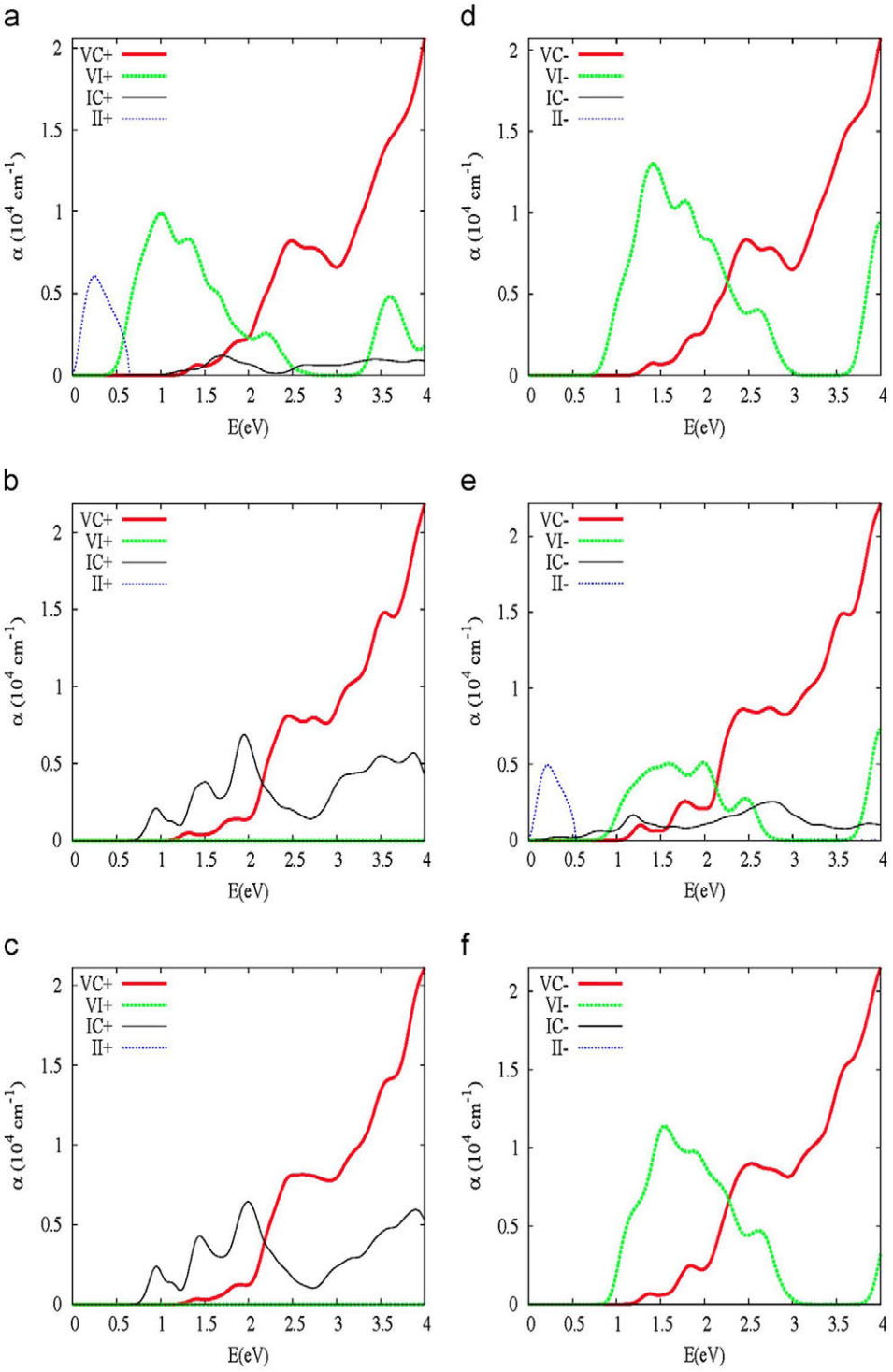

Fig. 3. Absorption coefficients for the transitions split between bands and between spin polarizations for the Ir_{Sn}, Ir_{Cu}, and Ir_{Zn} CZTS substitutions using the HLP. The transition between VB–IB, VB–CB, IB–CB and IB–IB are denoted in the figure by VI, VC, IC and II respectively. In addition, the (+) or (−) indicate the spin polarization. With this notation the panels represent: (a) $Ir_{Sn}(+)$, (b) $Ir_{Cu}(+)$, (c) $Ir_{Zn}(+)$, (d) $Ir_{Sn}(-)$, (e) $Ir_{Cu}(-)$, and (f) $Ir_{Zn}(-)$.

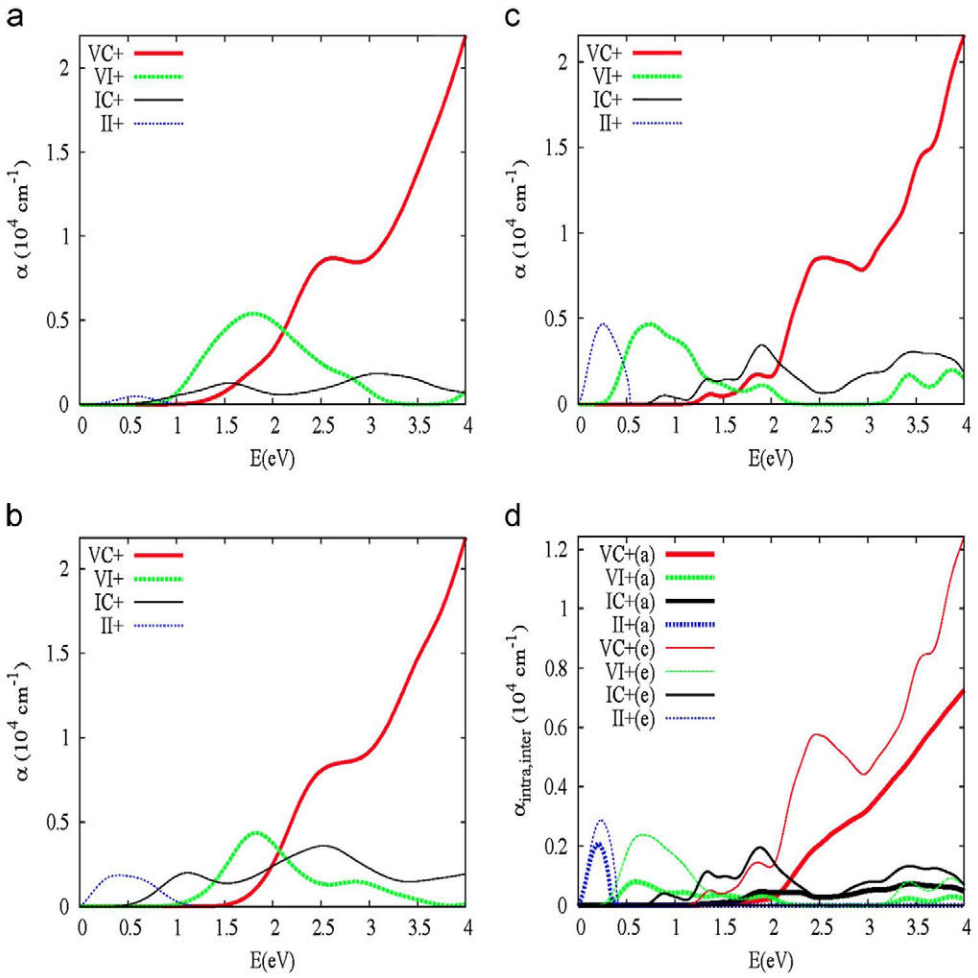

Fig. 4. (a) Absorption coefficients for the transitions between the VB and the IB (VI+ in the figure), the VB and the CB (VC+ in the figure), the IB and the CB (IC+ in the figure), and inside the IB (II+ in the figure) for the majority spin component of the (a) V_{Zn}, (b) V_{Cu} and (c) Cr_{Zn} substitutions using the HLP. (d) Absorption coefficients of (c) split in the intra (indicated with an (a) symbol and with thick lines) and inter components (indicated with an (e) symbol and with fine lines).

with the CB (panel b in Fig. 1). Nevertheless, because the IBs within the energy bandgap are very similar for all substitutions with HLP and SLP, except for the energetic position of the CB edge, these t_+-IB could be isolated from the CB if the GGA does not underestimate the bandgap. For the $Ir_{Cu}[t_+^3\, t_-^1]$ substitution, with a partially-full t_--IB something similar could happen.

The IBs in the band gap indicate the possibility of additional transitions between different bands, in addition to the VB–CB transition in the single gap semiconductors. Both the VB and CB edges of the CZTS have a large contribution from the p-S orbitals. As a consequence, the CZTS absorption coefficient is large. For the doped CZTS, the absorption coefficients for the more interesting cases have been calculated and broken down into the contributions from each type of transition and for each spin polarization. In Fig. 3 the absorption coefficients are shown for all Ir substitutions. The presence of an IB within host energy bandgap permits, additionally to the usual VB–CB transition, more photon absorption and emission channels depending on the IB occupation: if the IB is full there are IB–CB transitions; if it is empty, there are VB–IB transitions; and if it is partially full, there are VB–IB, IB–CB and IB–IB transitions. It is particularly interesting for the $V_{Cu}[t_+^2]$, $V_{Zn}[t_+^1]$, $Cr_{Zn}[t_+^2]$,$Ir_{Cu}[t_+^3\, t_-^1]$, and $Ir_{Sn}[t_+^1\, t_-^0]$ substitutions, with a partially-full IB. For the first three, the absorption coefficients are shown in Fig. 4.

For the substitutions with a partially-full IB, the current produced by photon absorption (electrons in CB and holes in VB) will be larger than in single-gap host semiconductors because the two-transition sub-gap (VB–IB and IB–CB) allows additional carrier generation from the VB to the CB by a two-photon process. Therefore the efficiency of solar cells based on these materials could be larger [23] than that based on the host semiconductor (conventional single-gap device). The IB–IB transitions do not significantly influence the operation of the solar cell. The external contacts are connected to the VB and the CB. Therefore, the IB does not contribute to the carrier transport (electrons in the CB and holes in the VB) extracted by the contacts. As has been previously mentioned, the IB is formed mainly through the combination of the d_t-M and the p-S host states, meaning that these sub bandgap absorptions are also relatively large.

In order to analyze the intra-atomic and inter-atomic contributions to the absorption coefficient we detail these separations for the $Cr_{Zn}[t_+^2]$ substitution with a partially full IB in Fig. 4d. Both inter- and intra-atomic components are important. In general, the inter-atomic component is larger than the intra-atomic. This is because both the VB, the CB and the IB have contributions from the p-S orbitals. In the IB case, the inter-atomic contribution confirms again that the IB has contributions from both the impurity d_t states and p-S states of the nearest neighbors.

4. Conclusions

Using first-principles methods, we studied the optoelectronic properties of M-doped CZTS at cation sites with M=V, Cr and Ir. In these analyses we have used the lattice cell parameters of both natural and synthetic CZTS. The electronic structure of these modified CZTS is

characterized in most of the substitutions for an IB in the gap. This IB is full, empty and partially full depending of the substitutions. It is particularly interesting for the $V_{Cu}[t_+^2]$, $V_{Zn}[t_+^1]$, $Cr_{Zn}[t_+^2]$,$Ir_{Cu}[t_+^3\,t_-^1]$, and $Ir_{Sn}[t_+^1\,t_-^0]$ substitutions, with a partially-full IB. This IB with t symmetry is made up mainly of a combination of the d_t-M and of the p_t-S states of the nearest neighbors to M atom. This t_+-IB allows additional photon absorption and emission channels depending on its occupation. When the t_+-IB is partially full, the additional VB–IB and IB–CB sub band gap transitions permit the absorption of lower energy photons than the host semiconductor. As a consequence, there is an increase in the number of carriers in the VB (electrons) and in the CB (holes). Therefore, the efficiency of the solar energy conversion could be increased with respect to the undoped host semiconductor.

Finally, the absorption coefficients have been obtained and split into inter-band transitions. They show an increase in light absorption below the host gap as a result of these additional absorption channels. These sub bandgap transition are significant because the p-S states have contribution to the VB, CB and IB. Therefore, these doped-CZTS could therefore be used for novel optoelectronic devices.

Acknowledgments

This work has been supported by the National Spanish PROMESA projects (ENE2012-37804-C01) and the European Commission through the funding of the project NGCPV (FP7-EU-JPN 283798).

References

[1] R.S. Hall, J.T. Szymanski, J.M. Stewart, Kesterite, Cu_2Zn,$FeSnS_4$, and stannite, Cu_2Fe,$ZnSnS_4$, structurally similar but distinct minerals, Can. Mineral 16 (1978) 131–137.
[2] S. Schorr, The crystal structure of kesterite type compounds: a neutron and X-ray diffraction study, Sol. Energy Mater. Sol. Cells 95 (2011) 1482–1488.
[3] N. Momose, M. Than Htay, T. Yudasaka, S. Igarashi, T. Seki, S. Iwano, Y. Hashimoto, K. Ito, Cu_2ZnSnS_4 thin film solar cells utilizing sulfurization of metallic precursor prepared by simultaneous sputtering of metal targets, Jpn. J. Appl. Phys. 50 (2011) 01BG09.
[4] H. Katagiri, Cu_2ZnSnS_4 thin film solar cells, Thin Solid Films 480–481 (2005) 426–432.
[5] T. Tanaka, T. Nagatomo, D. Kawasaki, M. Nishio, Q. Guo, A. Wakahara, A. Yoshida, H. Ogawa, Preparation of Cu_2ZnSnS_4 thin films by hybrid sputtering, J. Phys. Chem. Solids 66 (2005) 1978–1981.
[6] A. Weber, H. Krauth, S. Perlt, B. Schubert, I. Kotschau, S. Schorr, H.W. Schock, Multi-stage evaporation of Cu_2ZnSnS_4 thin films, Thin Solid Films 517 (2009) 2524–2526.
[7] N. Kamoun, H. Bouzouita, B. Rezig, Fabrication and characterization of Cu_2ZnSnS_4 thin films deposited by spray pyrolysis technique, Thin Solid Films 515 (2007) 5949–5952.
[8] H. Yoo, J. Kim, Comparative study of Cu_2ZnSnS_4 film growth, Sol. Energy Mater. Sol. Cells 95 (2011) 239–244.
[9] K. Tanaka, M. Oonuki, N. Moritake, H. Uchiki, Cu_2ZnSnS_4 thin film solar cells prepared by non-vacuum processing, Sol. Energy Mater. Sol. Cells 93 (2009) 583–587.
[10] T. Todorov, O. Gunawan, S.J. Chey, T. Goislard de Monsabert, A. Prabhakar, D. B. Mitzi, Progress towards marketable earth-abundant chalcogenide solar cells, Thin Solid Films 519 (2011) 7378–7381.
[11] A. Ennaoui, M. Lux-Steiner, A. Weber, D. Abou-Ras, I. Kotschau, H.-W. Schock, R. Schurr, A. Holzing, S. Jost, R. Hock, T. Vo, J. Schulze, A. Kirbs, Cu_2ZnSnS_4 thin film solar cells from electroplated precursors: novel low-cost perspective, Thin Solid Films, 517, 2511–2514.
[12] G.P. Bernardini, D. Borrini, A. Caneschi, F. Di Benedetto, D. Gatteschi, S. Ristori, M. Romanelli, EPR and SQUID magnetometry study of Cu_2FeSnS_4 stannite and Cu_2ZnSnS_4 kesterite, Phys. Chem. Miner. 27 (2000) 453–461.
[13] H. Matsushita, T. Maeda, A. Katsui, T. Takizawa, Thermal analysis and synthesis from the melts of Cu-based quaternary compounds Cu-III-IV-VI4 and Cu2-II-IV-VI4, J. Cryst. Growth 208 (2000) 416.
[14] H. Katagiri, N. Ishigaki, T. Ishida, K. Saito, Characterization of Cu_2ZnSnS_4 thin films prepared by vapor phase sulfurization, Jpn. J. Appl. Phys 40 (2001) 500–504;
J.-S. Seol, S.-Y. Lee, J.-C. Lee, H.-D. Nam, K.-H. Kim, Electrical and optical properties of Cu_2ZnSnS_4 thin films prepared by rf magnetron sputtering process, Sol. Energy Mater. Sol. Cells 75 (2003) 155–162.
[15] F. Di Benedetto, G.P. Bernardini, D. Borrini, W. Lottermoser, G. Tippelt, G. Amthauer, 57Fe-and 119Sn-Mossbauer study on stannite Cu_2FeSnS_4-kesterite Cu2ZnSnS4 solid solution, Phys. Chem. Miner 31 (2005) 683–690.
[16] S. Schorr, H.-J. Hoebler, M. Tovar, A neutron diffraction study of the stannite-kesterite solid solution series, Eur. J. Mineral 19 (2007) 65–73.
[17] J.J. Scragg, P.J. Dale, L.M. Peter, Towards sustainable materials for solar energy conversion: preparation and photoelectrochemical characterization of Cu_2ZnSnS_4, Electrochem. Commun. 10 (2008) 639.
[18] H. Katagiri, K. Jimbo, S. Yamada, T. Kamimura, W.S. Maw, T. Fukano, T. Ito, T. Motohiro, Enhanced conversion efficiencies of Cu_2ZnSnS_4-based thin film solar cells by using preferential etching technique, Appl. Phys. Express 1 (2008) 041201.
[19] K. Hönes, E. Zscherpel, J. Scragg, S. Siebentritt, Shallow defects in Cu_2ZnSnS_4, Physica B 404 (2009) 4949–4952.
[20] S. Chen, X.G. Gong, A. Walsh, S-H Wei, Crystal and electronic band structure of Cu_2ZnSnX_4 X=S and Se photovoltaic absorbers: first-principles insights, Appl. Phys. Lett 94 (2009) 041903.
[21] J. Paier, R. Asahi, A. Nagoya, G. Kresse, Cu_2ZnSnS_4 as a potential photovoltaic material: a hybrid Hartree–Fock density functional theory study, Phys. Rev. B: Condens. Matter 79 (2009) 115126.
[22] S. Chen, J-H Yang, X.G. Gong, A. Walsh, S-H Wei, Intrinsic point defects and complexes in the quaternary kesterite semiconductor Cu_2ZnSnS_4, Phys. Rev. B: Condens. Matter 81 (2010) 245204.
[23] C. Tablero, Effect of the oxygen isoelectronic substitution in Cu_2ZnSnS_4 and its photovoltaic application, Thin Solid Films 520 (2012) 5011.
[24] Z. Jun, S. LeXi, Cu_2ZnSnS_4 thin films prepared by sulfurizing different multi-layer metal precursors, Sci. China Ser E-Tech. Sci. 52 (2009) 269.
[25] A. Luque, A. Martí, Increasing the efficiency of ideal solar cells by photon transitions at intermediate levels, Phys. Rev. Lett 78 (1997) 5014–5017.
[26] C. Tablero, D. Fuertes Marrón, Analysis of the electronic structure of modified $CuGaS_2$ with selected substitutional impurities: prospects for intermediate-band thin-film solar cells based on Cu-containing chalcopyrites, J. Phys. Chem. C 114 (2010) 2756.
[27] C. Tablero, Ionization levels of doped sulfur and selenium chalcopyrites, J. Appl. Phys 106 (2009) 073718.
[28] C. Tablero, Electronic and magnetic properties of the Fe-doped $CuInS_2$, Chem. Phys. Lett 499 (2010) 75.
[29] C. Tablero, Ionization levels of doped copper indium sulfide chalcopyrites, J. Phys. Chem. A 116 (2012) 1390–1395.
[30] C. Tablero, Electronic and magnetic properties of ZnS doped with Cr, Phys. Rev. B: Condens. Matter 74 (2006) 195203.
[31] C. Tablero, Impurity–host interactions in Cr-substituted ZnSe, Solid State Commun 143 (2007) 399–402.
[32] B. Lee, L. Wang, Electronic structure of ZnTe:O and its usability for intermediate band solar cell, Appl. Phys. Lett 96 (2010) 071903.
[33] Y. Burki, P. Sshwendimann, W. Czaja, H. Berger, The temperature dependence of the photoluminescence and lifetime of ZnTe:O, J. Phys.: Condens. Matter 5 (1993) 9235–9252.
[34] Y. Burki, P. Sshwendimann, W. Czaja, H. Berger, Optical gain in ZnTe: O at 2 K, Europhys. Lett. 13 (1990) 555–559.
[35] C. Tablero, A. Martí, A. Luque, Analyses of the intermediate energy levels in ZnTe:O alloys, Appl. Phys. Lett. 96 (2010) 121104.
[36] J.L. Merz, Isoelectronic oxygen trap in ZnTe, Phys. Rev 176 (1968) 961–968.
[37] W.K. Ge, S.B. Lam, I.K. Sou, J. Wang, Y. Wang, G.H. Li, H.X. Han, Z.P. Wang, Sulfur forming an isoelectronic center in zinc telluride thin films, Phys. Rev. B: Condens. Matter 55 (1997) 10035–10039.
[38] M.J. Seong, H. Alawadhi, I. Miotkowski, A.K. Ramdas, S. Miotkowska, Oxygen isoelectronic impurity in ZnS_xTe_{1-x}, Phys. Rev. B: Condens. Matter 60 (1999) R16275–R16278.
[39] Y.M. Yu, S. Nam, K.-S. Lee, Y. Dae Choi, O. Byungsung, Photoluminescence characteristics of ZnTe epilayers, J. Appl. Phys. 90 (2001) 807.
[40] W. Wang, A.S. Lin, J.D. Phillips, W.K. Metzger, Generation and recombination rates at ZnTe:O intermediate band states, Appl. Phys. Lett. 95 (2009) 261107.
[41] L.D. DeLoach, R.H. Page, G.D Wilke, S.A. PayneW.P. Krupke, Transition metal-doped zinc chalcogenides: spectroscopy and laser demonstration of a new class of gain media, IEEE J. Quantum Electron. 32 (1996) 885–895.
[42] R.H. Page, K.I. Schaffers, L.D. DeLoach, G.D. Wilke, F.D. Patel, J.B. Tassano, S. A. Payne, W.F. Krupke, K.T. Chen, A. Burger, Cr^{2+}-doped zinc chalcogenides as efficient, widely tunable mid-infrared lasers, IEEE J. Quantum Electron. 33 (1997) 609–619.
[43] I.T. Sorokina, Cr^{2+}-doped II–VI materials for lasers and nonlinear optics, Opt. Mater 26 (2004) 395.
[44] W. Kohn, L.J. Sham, Self-consistent equations including exchange and correlation effects, Phys. Rev 140 (1965) A1133–A1138.
[45] J.M. Soler, E. Artacho, J.D. Gale, A. García, J. Junquera, P. Ordejon, D. Sánchez-Portal, The SIESTA method for ab initio order-N materials simulation, J. Phys.: Condens. Matter 14 (2002) 2745–2779.
[46] J.P. Perdew, K. Burke, M. Ernzerhof, Generalized gradient approximation made simple, Phys. Rev. Lett. 77 (1996) 3865–3868.
[47] N. Troullier, J.L. Martins, Efficient pseudopotentials for plane-wave calculations, Phys. Rev. B: Condens. Matter 43 (1991) 1993–2003.
[48] L. Kleinman, D.M. Bylander, Efficacious form for model pseudopotentials, Phys. Rev. Lett. 48 (1982) 1425–1428;
D.M. Bylander, L. Kleinman, 4f Resonances with norm-conserving pseudopotentials, Phys. Rev. B: Condens. Matter 41 (1990) 907–912.
[49] O.F. Sankey, D.J. Niklewski, Ab initio multicenter tight-binding model for molecular-dynamics simulations and other applications in covalent systems, Phys. Rev. B: Condens. Matter 40 (1989) 3979–3995.
[50] C. Tablero, Electronic and photon absorber properties of Cr-doped Cu_2ZnSnS_4, J. Phys. Chem. C 116 (2012) 23224–23230.